Article

Diesel soot photooxidation enhances the heterogeneous formation of H_2SO_4

Peng Zhang[1], Tianzeng Chen[1,2], Qingxin Ma [1,2,3] ✉, Biwu Chu [1,2,3], Yonghong Wang[1,2], Yujing Mu [1,2,3], Yunbo Yu[1,2,3] & Hong He [1,2,3] ✉

Both field observation and experimental simulation have implied that black carbon or soot plays a remarkable role in the catalytic oxidation of SO_2 for the formation of atmospheric sulfate. However, the catalytic mechanism remains ambiguous, especially that under light irradiation. Here we systematically investigate the heterogeneous conversion of SO_2 on diesel soot or black carbon (DBC) under light irradiation. The experimental results show that the presence of DBC under light irradiation can significantly promote the heterogeneous conversion of SO_2 to H_2SO_4, mainly through the heterogeneous reaction between SO_2 and photo-induced OH radicals. The detected photochemical behaviors on DBC suggest that OH radical formation is closely related to the abstraction and transfer of electrons in DBC and the formation of reactive superoxide radical ($\cdot O_2^-$) as an intermediate. Our results extend the known sources of atmospheric H_2SO_4 and provide insight into the internal photochemical oxidation mechanism of SO_2 on DBC.

The rapid increase in vehicle numbers has resulted in the emission of large quantities of black carbon (BC) into the lower atmosphere[1–4]. BC particles in vehicle exhaust are mainly formed by incomplete combustion of hydrocarbon fuels[5–7]. In particular, in northern China, BC mass concentrations of up to $20\,\mu g\,m^{-3}$ (nearly 10% of the total particulate matter) have been observed during haze episodes[8]. High loading of BC can increase atmospheric stability through the formation of a temperature inversion, which will feed back to the development of extreme haze via suppressing air pollutant dispersion[9]. Moreover, BC aerosol can influence climate by directly absorbing solar radiation and affecting cloud formation and surface albedo through deposition on snow and ice[10–15].

Recent works proved that the interactions between BC and other inorganic species can enhance the atmospheric oxidation capacity and contribute to the formation of complex air pollution[16,17]. For instance, gaseous nitrous acid (HONO) is an important precursor of hydroxyl radical (OH) in the troposphere. Numerous studies have shown that the heterogeneous reduction of NO_2 on the BC surface is an important HONO source[18–22]. Moreover, sulfate is the fastest-forming species and rapidly becomes the main component of secondary aerosols during the

evolution of haze[23–28]. Recent laboratory simulation and theoretical calculation works have indicated that soot can act as a catalyst to promote the heterogeneous oxidation of SO_2 to sulfate under dark conditions[29–31]. Chamber experiments also proved that the catalytic role of soot in sulfate formation can be further amplified by reducing NO_2 to HONO in the presence of both NO_2 and NH_3 under dark conditions[32]. A recent field measurement in urban Beijing conducted by Yao et al. indicated that the catalytic oxidation of SO_2 on traffic-related soot can induce the formation of gas-phase SO_3 in the early morning[33]. Therefore, the heterogeneous chemistry involving soot has recently attracted increasing attention in the field of atmospheric chemistry.

Relative to its role under dark conditions, some recent studies reported that both elemental carbon (EC) and organic carbon (OC) in BC exhibited conspicuous photo-reactivity due to their strong light absorption capability under illumination[19,34–37]. The EC-initiated photooxidation of OC was found to proceed through radical reactions initiated by electron transfer, and the absorption of light by OC-induced direct photoaging by energy transfer. Recent observational evidence suggested that photochemical reactions on soot particles may contribute to the production of atmospheric sulfate during the daytime[38].

[1]State Key Joint Laboratory of Environment Simulation and Pollution Control, Research Center for Eco-Environmental Sciences, Chinese Academy of Sciences, 100085 Beijing, China. [2]University of Chinese Academy of Sciences, 100049 Beijing, China. [3]Center for Excellence in Regional Atmospheric Environment, Institute of Urban Environment, Chinese Academy of Sciences, 361021 Xiamen, China. ✉e-mail: qxma@rcees.ac.cn; honghe@rcees.ac.cn

However, the intrinsic reaction mechanism of SO_2 on BC remains poorly resolved. Moreover, whether photoinduced radical chemistry can contribute to the heterogeneous conversion of SO_2 remains unclear.

In this work, a series of laboratory experiments are conducted to explore the underlying SO_2 oxidation mechanism on soot particles emitted from diesel vehicles (DBC) under light irradiation. In-situ diffuse reflectance infrared Fourier transform spectroscopy (DRIFTS) measurements and thermogravimetric analysis mass (TGA–MS) analysis are applied to characterize the formation of surface H_2SO_4 on DBC under light irradiation. Combined with the reactive oxygen species (ROS) analysis from electron spin resonance (ESR), it is found that OH radical resulting from the conversion of superoxide radicals is the crucial oxidant during the heterogeneous conversion of SO_2 to H_2SO_4. These results help in understanding the sources of atmospheric oxidation capacity and particulate H_2SO_4.

Results

Formation and characterization of sulfur-containing products on DBC surface

The composition and structure of DBC were firstly analyzed and characterized using in-situ DRIFTS, XPS, and XRD methods. The detailed characterization results for DBC are shown in Fig. S1. In brief, DBC was found to be amorphous and highly graphitized. Various oxygen-containing groups (such as C=O, C–OH, and C–O–C) were detected in DBC through FTIR and XPS analysis.

Heterogeneous conversion of SO_2 on the DBC surface was systematically investigated using in-situ DRIFTS. The main peak at 1100 cm^{-1} represents the characteristic vibrations of S=O bonds in sulfur-containing products (Fig. 1a)[39]. The significant increase in peak intensity with reaction time indicated that the heterogeneous reaction between SO_2 and DBC resulted in the production and gradual accumulation of sulfur-containing products. As shown in Fig. 1b, c, both the presence of DBC and light irradiation can remarkably promote the heterogeneous formation of sulfur-containing species compared to reaction under dark conditions and in blank experiments. This implies that the remarkable heterogeneous conversion of SO_2 to sulfur-containing species should be closely related to the photo-induced catalytic role of DBC. From Fig. S2, the observation of similar in-situ DRIFTS experimental results implies that DBC photooxidation would most likely promote the heterogeneous oxidation of SO_2 under low-level SO_2 conditions (~1 ppm).
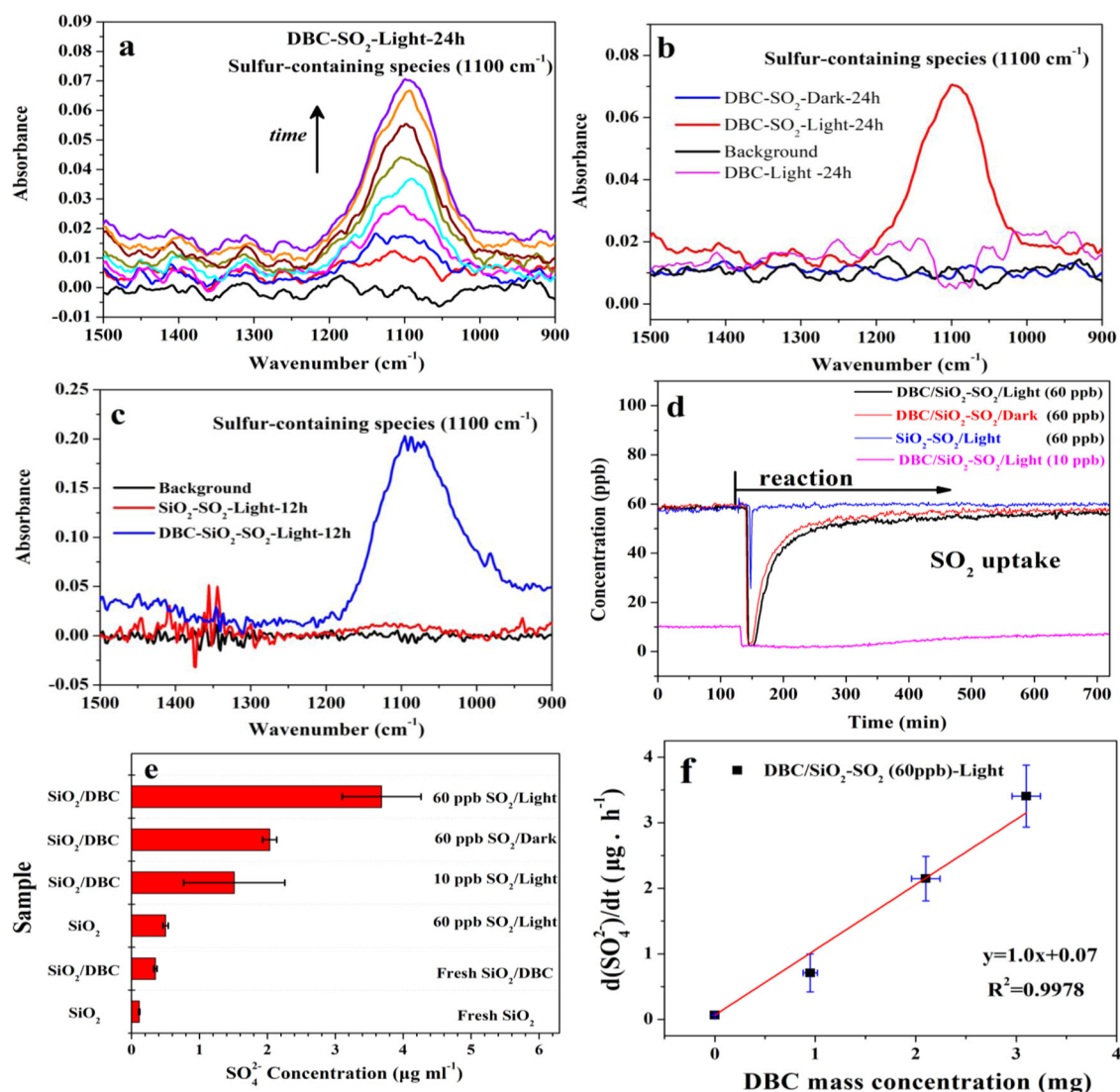

Fig. 1 | Formation and yield of sulfur-containing products on DBC surface. In-situ DRIFTS spectra of DBC exposed to 10 ppm SO_2 for 24 h under irradiation (**a**); comparison of sulfur-containing species formation under light and dark conditions (**b**); comparison of sulfur-containing species formation in the absence and presence of DBC under light irradiation (**c**); SO_2 uptake on DBC (0.002 g)/SiO_2(1 g) and SiO_2(1 g) under different conditions (**d**); comparison of H_2SO_4 concentrations under different conditions (**e**); H_2SO_4 formation rate as a function of DBC concentration (**f**). Error bars represent standard deviation.

Considering that typical atmospheric concentrations of SO_2 are at the ppb level (Fig. S3), the heterogeneous conversion of SO_2 (10 and 60 ppb) on the DBC surface was carried out in a tube plug flow reactor (Fig. S4). Figure 1d shows the uptake curves of 60 and 10 ppb SO_2 on DBC/SiO_2 or SiO_2 particles. It was found that the uptake of SO_2 (60 ppb) on DBC/SiO_2 mixtures is much greater than that on SiO_2. Moreover, the uptake of 10 ppb SO_2 on DBC is also observed to last more than 10 h under light irradiation. These results indicate that the heterogeneous uptake of SO_2 on DBC is significant even under conditions close to the real atmosphere. The comparison of extracted SO_4^{2-} ions from different samples (Fig. 1e) further highlights the enhancing role of DBC on the heterogeneous oxidation of SO_2 under both dark conditions and light irradiation. The formation of SO_4^{2-} under dark conditions may be due to the catalytic oxidation of SO_2 on the surface-active site of soot as reported in previous studies[30,33]. The SO_4^{2-} concentrations obtained under light irradiation are much higher than those under dark conditions. This is in consistent with DRIFTS results and further proved the role of DBC in photocatalytic oxidation of SO_2 under conditions close to the real atmosphere. To obtain the formation rates of sulfur-containing species on DBC, photooxidation experiments of SO_2 (~60 ppb) on DBC of different masses were also carried out (Fig. S5). The measured formation rates of sulfur-containing species varied linearly with the mass concentration of DBC under light irradiation, and the mass normalization rate was determined to be ~1.0×10^{-3} µg h^{-1} (Fig. 1f). On this basis, the formation rates of sulfur-containing products in the wintertime in Beijing due to the photooxidation of SO_2 on BC could be estimated to be in the range of 0.01–0.018 µg m^{-3} h^{-1} according to the observed BC mass concentrations (10.4–17.8 µg m^{-3})[32]. This is comparable with the reported formation rate of gaseous H_2SO_4 (~0.001–0.1 µg m^{-3} h^{-1}) from the OH reaction pathway[27]. These results suggest that the photooxidation of SO_2 on BC could be an important source of sulfate in areas with high BC loading.

To further reveal the form of sulfur species on the DBC surface, several characterization techniques were employed. Given that trace amounts of metal elements that can act as catalysts may break off from the NO_X selective catalytic reduction catalyst in diesel after-treatment systems and be emitted along with DBC, we investigated the elemental composition of DBC by XPS. From the survey XPS spectrum of DBC shown in Fig. S6, metallic elements were hardly detected in the DBC. This also implied that the sulfur-containing species detected were not metal sulfates, due to the lack of positive ions containing such metal elements. Thus, we speculated that the photooxidation of SO_2 on DBC mainly produces H_2SO_4 or sulfur-containing organics rather than metal sulfate complexes.

The pH measurement results in Fig. 2a show that the pH of SO_2–aged DBC (~2.68) was apparently lower than that of fresh DBC (~3.74), which suggested that H_2SO_4 was formed in the photooxidation reaction on DBC. To confirm the formation of particulate H_2SO_4, TGA−MS was employed to characterize H_2SO_4 on aged-DBC[40–42]. From the TGA−MS of aged-DBC, a saddle-like change in SO_2 (m/z 64 in Fig. 2b) and SO (m/z 48 in Fig. S7) fragments were observed in the temperature intervals of 200–400 and 400–600 °C, respectively. According to the evolution of water and sulfur-containing fragments in the TGA−MS of pure H_2SO_4 (Fig. S8), it could be found that the evaporation and pyrolysis of H_2SO_4 occur in the temperature range of 200–400 °C. Thus, the formation of SO_2 fragments between 200 and 400 °C in the TGA−MS of SO_2-aged DBC proved that H_2SO_4 exists in SO_2–aged-DBC. The SO_2 fragments in the range 400–600 °C should be derived from other sulfur-containing species such as H_2SO_4–graphite intercalation compounds (H_2SO_4-GIC, $(C_{24}^+(HSO_4^-)(H_2SO_4)_2)_n)$). Previous studies proved that the pyrolysis of H_2SO_4–GIC could produce SO_2 fragments in the range 400–600 °C[43,44]. Furthermore, the similar formation and evolution of sulfur-containing fragments in TGA−MS of a H_2SO_4–DBC mixture (30 µL H_2SO_4 and 15 mg DBC) further support
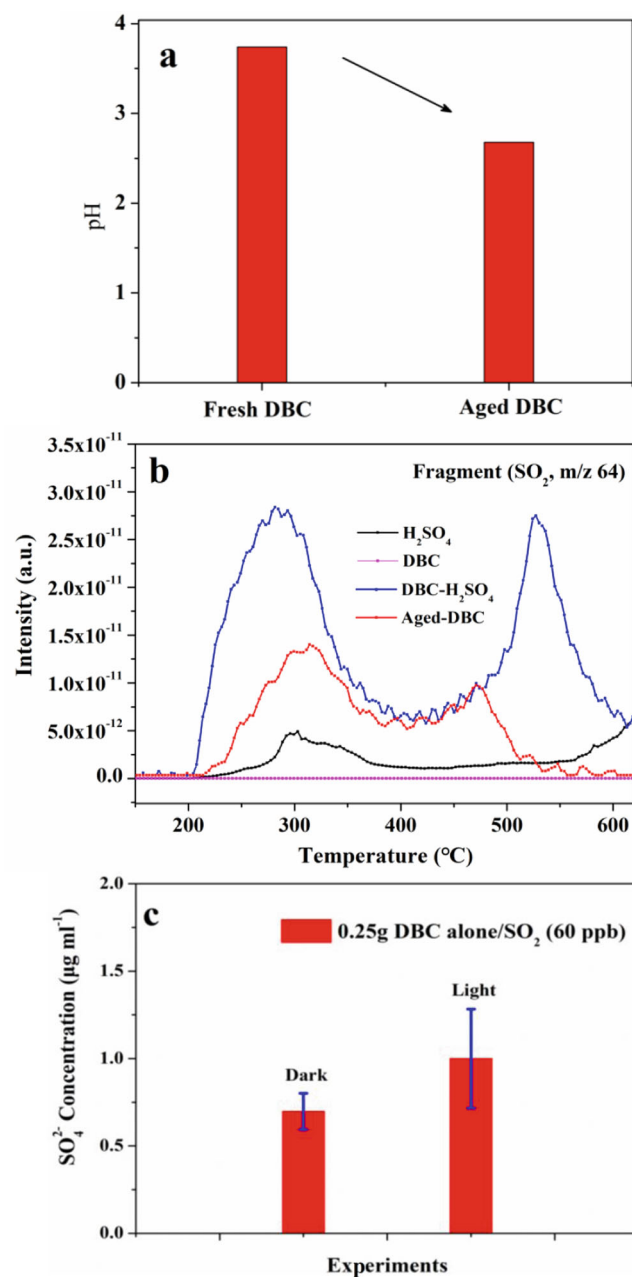

Fig. 2 | Characterization of H_2SO_4 on DBC surface. pH values of fresh DBC and SO_2-aged DBC (**a**). Evaluation and comparison of sulfur-containing fragments (**b**). The comparison of captured gaseous H_2SO_4 under dark and light irradiation. Error bars represent standard deviation (**c**).

the supposition that the interaction between DBC and H_2SO_4 can produce some other sulfur-containing species (Fig. 2b).

Recent work reported that the soot surfaces upon irradiation can give rise to gaseous OH radicals[45]. It can be speculated that these photoinduced OH radicals may react with SO_2 to form gaseous H_2SO_4. Thus, to confirm the formation of gaseous H_2SO_4, the gaseous products of the photochemical reaction of SO_2 on DBC in a quartz photoreaction flow tank (Fig. S9) were captured using formaldehyde solution (4 ml, 11% v/v). As shown in Fig. 2c, the concentration of SO_4^{2-} ions (1.0 ± 0.28 µg ml^{-1}) after 24 h reaction under light irradiation was greater than that (0.7 ± 0.1 µg ml^{-1}) under dark conditions. This further provided convincing evidence for the formation of gaseous H_2SO_4. The condensation of gaseous H_2SO_4 could be a source of surface H_2SO_4.

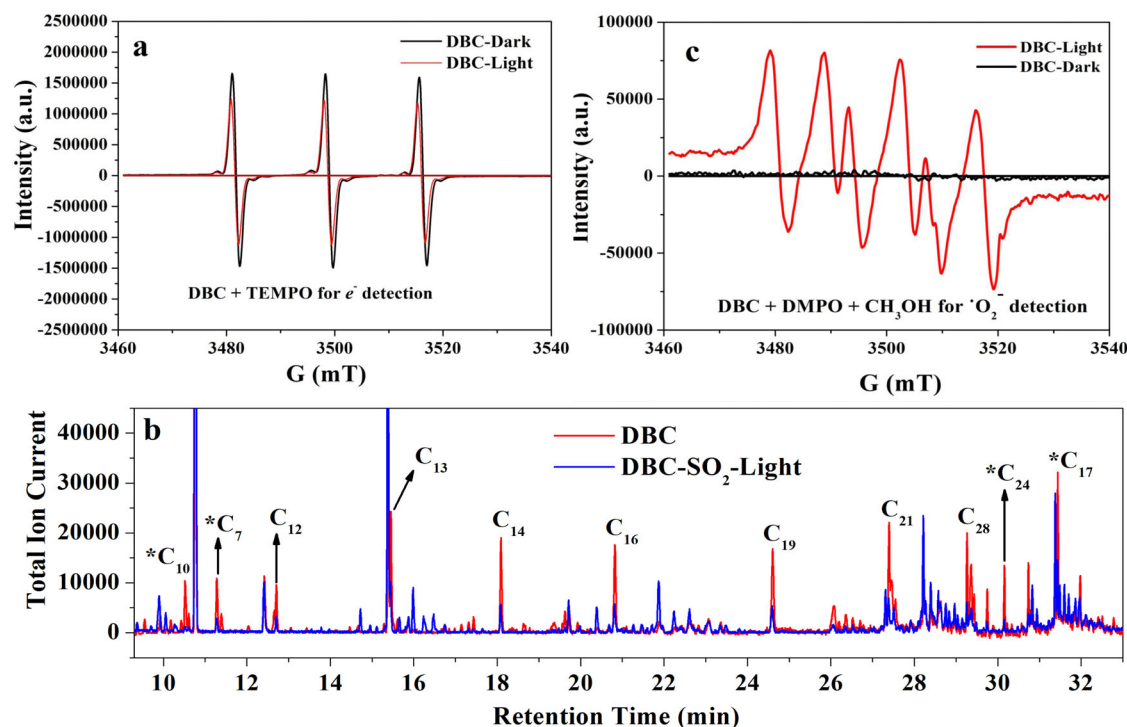**Fig. 3 | Reactive intermediates on DBC under light irradiation.** TEMPO spin-trapping ESR spectra for the detection of electrons in DBC suspension (**a**). Comparison of OC signals from fresh DBC and DBC aged by SO_2 under light irradiation, *C represents aromatic hydrocarbon with different functional groups (such as methyl, oxygen, and chlorine) (**b**). DMPO spin-trapping ESR spectra for the detection of $•O_2^-$ in DBC suspension with methanol (CH_3OH) under dark and light irradiation conditions (**c**).

Heterogeneous formation pathway of H_2SO_4

A recent work by Li et al. proved that the EC-initiated photooxidation of soot mainly involves electron transfer and the formation of reactive oxygen species[34]. To shed light on the mechanism of DBC photocatalysis in SO_2 oxidation, we also examined the generation of photo-induced electrons and reactive oxygen radicals during DBC photooxidation by the spin-trapping EPR technique. TEMPO was used as the spin-trapping agent for photo-induced electrons. As shown in Fig. 3a, the ESR spectrum of a DBC suspension with TEMPO showed a characteristic signal of three peaks with an intensity pattern of 1:1:1, representing the radical spin-label of TEMPO. It is worth noting that the signal intensity of the TEMPO radical decreased once exposed to light irradiation, demonstrating that TEMPO was partially reduced to an ESR-silent molecule such as TEMPOH by photo-induced electrons[46,47]. The conversion of TEMPO to TEMPOH indirectly indicated that DBC photooxidation can indeed induce the generation and transfer of electrons.

Li et al. reported that OC in soot is the major donor of electrons during soot photoaging[34]. To verify this, the OC in DBC was extracted and further analyzed by GC-MS. The results of GC-MS (Fig. 3b) showed that OC extracts from DBC mainly consist of saturated long-chain saturated alkanes with more than 10 carbons, and aromatic hydrocarbons with different functional groups (such as methyl, oxygen, and chlorine). It is worth noting that the relative signal intensity of OC significantly decreased after DBC was photoaged under light irradiation. This indicated that light irradiation should result in the photooxidation of OC in DBC and also implied that OC maybe the crucial donor of electrons during DBC photooxidation. However, it should be noted that there was almost no absorbance in the range of 200–800 nm for extracted OC as determined by diffuse reflectance UV–vis spectroscopy (Fig. S10b). This indicated that the long-chain saturated alkanes could not directly donate electrons under light irradiation. In contrast to OC, EC in DBC distinctly adsorbed radiation over a broad wavelength range from 200 to 800 nm (Fig. S10b).

Several studies reported that carbonaceous materials excited under light irradiation can induce the formation of surface electron−hole pairs, especially for these surfaces with plentiful surface structure defects and oxygen functional groups[37,48,49]. Given that various oxygen functional groups and structural defects or disordered structures are ubiquitous on carbonaceous materials in DBC (Figs. S1a and S11), the formation of photo-generated holes (h^+) on excited EC may abstract electrons from OC and subsequently donate electrons to other available acceptors such as adsorbed O_2 (Eq. (3))[50–53]. To further verify this, the photo-induced electron−hole pairs in residual EC were analyzed using TEMPO spin-trapping ESR spectra. As shown in Fig. S12, the remarkable decrease in the signal intensity of TEMPO radicals after 120 min light irradiation further demonstrates that the residual EC from DBC can indeed induce the generation of holes or electrons (Eq. (1)). Thus, long-chain saturated alkanes in DBC can indirectly donate electrons to absorbed O_2 via excited EC (Eqs. (2) and (3)) and subsequently be oxidized to other organic oxygen-bearing compounds (Eq. (4))[34].

To verify whether the observed photogenerated electrons can further result in the formation of reactive oxygen radicals ($•O_2^-$ and OH radical), we chose two spin traps, DMPO and BMPO, to capture $•O_2^-$ and OH radical, respectively. As shown in Fig. 3c, four characteristic peaks of DMPO−$•O_2^-$ adducts were observed in a DBC suspension in methanol under light irradiation, while no signal was observed under dark conditions[54]. This demonstrated that electrons were transferred to the dissolved O_2 in the DBC suspension, resulting in the formation of $•O_2^-$ radical (Eq. (3)). Previous studies reported that $•O_2^-$ radicals can interact with SO_2 or sulfite ion (SO_3^{2-}) to form a series of sulfur-containing radicals ($SO_3^{•-}$, $SO_5^{•-}$, and $SO_4^{•-}$)[55–57]. The free radical chain reaction dominated by sulfur-containing radicals would eventually result in sulfate formation. However, it should be noted that these sulfur-containing radicals are scarcely detected in the BMPO spin-trapping ESR spectra of SO_2-aged DBC (Fig. 4a) according to the reported measurement methods[58,59]. Thus, the contribution of the
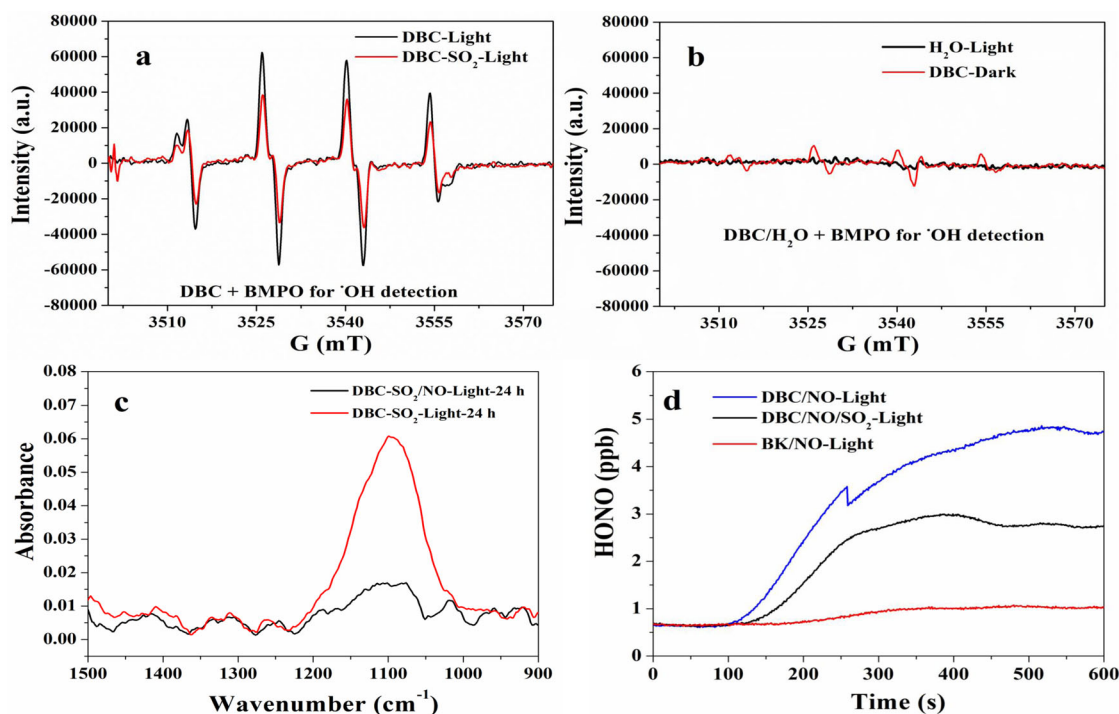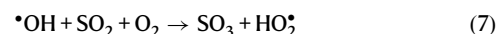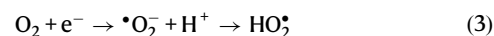
Fig. 4 | Photo-induced OH radical promoting the heterogeneous conversion of SO_2 to H_2SO_4. BMPO spin-trapping ESR spectra for the detection of OH radical in DBC suspension under light irradiation (**a**). BMPO spin-trapping ESR spectra for the detection of OH radical in DBC suspension in the dark and in water under light irradiation (**b**). Comparison of in-situ DRIFTS spectrum of sulfate in the absence and presence of 10 ppm NO (**c**). The heterogeneous conversion of NO (168 ppb) to HONO under different conditions (**d**).

heterogeneous reaction between SO_2 and $•O_2^-$ to H_2SO_4 should be limited despite the fact that this reaction may occur in this system.

In addition to its direct oxidation capability, $•O_2^-$ radical is also the key intermediate species in OH radical production during photo-induced interfacial reactions; thus, OH radicals in DBC suspension were further measured via the spin trapping EPR technique[46,60]. As shown in Fig. 4a, a significant signal of BMPO−OH adducts with a typical 1:2:2:1 quartet signal was observed, indicating that light irradiation could indeed cause the formation of OH radicals in the suspension of fresh DBC and DBC aged by SO_2. Almost no BMPO−OH adduct signals were observed in DBC under dark conditions or in ultrapure water under light (Fig. 4b). This further indicated that OH radical formation was closely related to the presence of DBC and light irradiation. These results proved that the photooxidation process of DBC indeed involves a complex electron transfer pathway and results in the generation of reactive oxygen radicals such as OH radicals (Eqs. (3), (5), and (6)). Moreover, the BMPO−OH adduct detected in aged-DBC treated with SO_2 apparently decreased relative to that in fresh DBC (Fig. 4a). This implied that the heterogeneous conversion of SO_2 to H_2SO_4 (Eqs. (7) and (8)) should be related to the consumption of OH radical from DBC. To further confirm this, the heterogeneous conversion of SO_2 on DBC under light irradiation was also investigated in the presence of high-level NO (radical scavenger). From the results of in-situ DRIFTS experiments shown in Fig. 3c, the presence of high-level NO (10 ppm) could significantly suppress the heterogeneous formation of H_2SO_4 on DBC. Moreover, the results of experiments in a coated-wall quartz flow tube reactor also showed that the presence of DBC indeed can promote the conversion of NO to HONO under light irradiation relative to the control experiment. Furthermore, the addition of SO_2 can also in turn hamper the heterogeneous conversion of NO to HONO (Fig. 4d). These results supported the hypothesis that the competing reactions of SO_2 + OH and NO + OH must exist during DBC photooxidation. This also proves that the heterogeneous oxidation of SO_2 by OH radicals should be an important formation pathway of

particulate H_2SO_4 on DBC under light irradiation.

$$EC \xrightarrow[\text{excited}]{h\nu} h^+ + e^- \tag{1}$$

$$OC + h^+ \rightarrow OC^+ \tag{2}$$

$$O_2 + e^- \rightarrow {}^\bullet O_2^- + H^+ \rightarrow HO_2^\bullet \tag{3}$$

$$OC^+ + {}^\bullet O_2^- / {}^\bullet OH \rightarrow \text{Carbonyl or others} \tag{4}$$

$$2HO_2^\bullet \rightarrow O_2 + H_2O_2 \tag{5}$$

$$H_2O_2 \xrightarrow{h\nu} 2{}^\bullet OH \tag{6}$$

$${}^\bullet OH + SO_2 + O_2 \rightarrow SO_3 + HO_2^\bullet \tag{7}$$

$$SO_3 + H_2O \rightarrow H_2SO_4 \tag{8}$$

Discussion

The conventional view recognizes BC particles as a reducing agent in the atmosphere. For example, BC was found to initiate the hetero-geneous reduction of NO_2 to HONO and hence elevate the atmo-spheric oxidation capacity in the atmosphere[19,20,22]. In this work, our experimental results indicated that DBC under light irradiation can act as an oxidation medium to directly promote the heterogeneous oxi-dation of SO_2 to H_2SO_4. Moreover, it was also proven that the pro-moting role of DBC photochemistry on the rapid conversion of SO_2 is linked to the photo-induced formation of OH radicals. As for the

source of OH radicals on soot under light irradiation, He et al. proposed that these OH radicals mainly derive from the reaction of photoinduced singlet oxygen (^1O) and H_2O on soot based on the density functional theory (DFT) results[45]. In this study, we found that the formation of OH radical is also closely related to the formation and conversion of the intermediate reactive superoxide radical ($\cdot O_2^-$) triggered by the abstraction and transfer of photoinduced electrons. Thus, our work further complements or improves the production mechanism of OH radicals on DBC under light irradiation, which provides insight into the photochemical reaction process on DBC.

H_2SO_4 in the atmosphere mainly comes from the reaction of SO_3 and H_2O, which is the critical precursor causing the rapid nucleation and growth of ultra-fine particle[61,62]. Thus, exploring the unknown sources of SO_3 and H_2SO_4 is crucial for understanding the formation and growth of new particles. Recently, both DFT calculation and field observation indicated that the formation of gaseous SO_3 during the early morning is closely related to the catalytic oxidation of SO_2 on the surface of soot[30,31,33]. Another field observation by Zhang et al. found that the photooxidation of BC-containing particles can further enhance the formation of sulfate[38]. Here, our experimental results provide reliable experimental evidence for these recent observations and DFT calculation results, especially under light irradiation. Hence, the heterogeneous oxidation of SO_2 to H_2SO_4 driven by the photochemical process on DBC may very directly contribute to the rapid formation and growth of new particles in the atmosphere via inducing the formation of gaseous and particulate H_2SO_4. Our study highlights the photooxidation role of DBC in the heterogeneous formation of H_2SO_4, which has important atmospheric implications for understanding new particle formation and the source of atmospheric sulfate. It was worth noting that further model simulation and field observation in future studies should be effectively combined to quantitatively evaluate the contribution of this new pathway to H_2SO_4 formation in the atmosphere.

Additionally, black carbon has strong effects on regional and global climate due to the remarkable positive (warming) radiative forcing in the atmosphere[63–65]. In particular, the internal mixing between BC and other aerosol components through processes such as gas condensation and coagulation can remarkably affect light absorption by BC[12,66,67]. This work proved that the photooxidation of DBC could directly promote the heterogeneous conversion of SO_2 to H_2SO_4. Thus, an in-depth study of the optical properties of BC aerosol internally mixed with sulfuric acid in the future will help to evaluate the effect of variation of the mixing state on direct radiative forcing and climate.

Methods

Experimental procedure

Diesel soot was collected from the diesel particle filter (DPF) of a China VI heavy-duty diesel engine (ISUZU from China). A diesel engine bench test was run under the conditions of the World Harmonized Transient Cycle (WHTC). China VI fuels were used in this study, meeting the GB T32859-2016 standard. The heterogeneous reactions of SO_2 or SO_2/NO on diesel soot particles were measured by in-situ DRIFTS (NEXUS 6700, Thermo Nicolet Instrument Corporation), equipped with a diffuse reflection chamber and a high-sensitivity mercury cadmium telluride (MCT) detector. The MCT was cooled by liquid N_2 prior to the measurement. The infrared spectra were collected by means of a computer using OMNIC 6.0 software (Nicolet Corporation, USA). All spectra reported here were recorded at a resolution of $4\ cm^{-1}$ for 100 scans in the spectral range $4000–650\ cm^{-1}$. The spectra are presented in the Kubelka−Munk (K−M) scale, which can provide a better linear relation with concentration via reducing or eliminating the mirror effect. To simulate solar irradiation, a high uniformity integrated xenon lamp (PLS-FX300HU, Beijing Perfectlight Technology Co., Ltd.) was used as the light source[34]. Its visible spectrum ranges from 330 to 850 nm (Fig. S10a). The light in the near-infrared and infrared bands was filtered

using a transmission-reflection filter (VISREF). DBC was placed into a cylindrical ceramic crucible in the diffuse reflection chamber before DRIFTS measurement. Before the reaction, the DBC was purged with $200\ mL\ min^{-1}$ air at 298 K and 55% RH until the infrared spectrum was unchanged. Then the samples were exposed to 10 ppm SO_2 balanced with $200\ mL\ min^{-1}$ synthetic air for at least 12 h.

The experiments on HONO detection were conducted in a coated-wall quartz flow tube reactor (34 cm length, 1.6 cm i.d.)[68,69]. The coated tube with the deposited DBC sample was horizontally placed in the main reactor. Synthetic air, as the carrier gas, introduced NO and SO_2 into the coated flow tube at a total flow rate of $2\ L\ min^{-1}$. Inorganic gases (SO_2 and NO) were introduced into the flow tube through a movable injector with 0.3 cm radius. HONO was measured by a long-path absorption photometer (HONO-1000, Beijing Zhichen Technology Co. Ltd), while the reactant gas SO_2 in the coated flow tube was measured by a Thermo Scientific analyzer (43i SO_2 analyzer). To better simulate the heterogeneous conversion of SO_2 on DBC under close-to-atmosphere conditions, heterogeneous experimental tests with low SO_2 concentrations (∼60 and 10 ppb) were further carried out in a quartz tube plug flow reactor (40 cm in length, 0.6 cm in diameter) at 37% RH. Before loading the sample into the plug flow reactor, ∼2 mg DBC needed to be diluted using ∼1 g silica sand (analytically pure, 1–2 mm in diameter) to ensure the reaction gas could flow fluently through the DBC. To further verify that DBC photooxidation in the presence of SO_2 could also promote the formation of gaseous H_2SO_4, the heterogeneous reaction of SO_2 (∼60 ppb) on DBC (∼0.25 g) powder alone was carried out in a quartz photoreaction tank at 50% RH. Prior to the reaction, 0.25 g DBC power was uniformly dispersed into a shallow quartz vessel (7 cm in diameter and 0.4 cm in depth) and then placed into the photoreaction tank. The outlet of the quartz photoreaction tank was connected with a quartz trap bottle (2 cm in diameter and 7 cm in depth) with 4 ml formaldehyde solution (20% v/v). Gaseous H_2SO_4 from the interaction between SO_2 and DBC was captured using ultrapure water in the quartz trap. The captured H_2SO_4 was analyzed using IC. The designed RH in the DRIFTS chamber or in the flow tube was obtained by varying the ratio of dry zero air to wet zero air. A flow of humid vapor was generated by bubbling zero air through ultrapure water. A Vaisala HMP110 probe was used to monitor the changes in RH online.

DBC characterization

Surface chemical states were analyzed by X-ray photoelectron spectrometry (XPS) (ESCALAB 250Xi, Thermo Scientific). An X-ray powder diffractometer (Bruker D8 ADVANCE 2θ diffractometer) with Cu Kα radiation ($\lambda = 0.15406$ nm) operated at 40 kV and 40 Ma was used to characterize the crystalline form and interlayer spacings of the DBC power. The patterns were measured over the 2θ range from 10° to 80° with a scanning step size of 0.02°. The OC in DBC was analyzed and identified via gas chromatography coupled with mass spectrometry (GC−MS, Agilent 6890−5973). DBC was first ultrasonically extracted for 10 min using 20 ml of dichloromethane (CH_2Cl_2), which was filtered through a quartz sand filter. The obtained supernatant liquid was subsequently concentrated using the N_2 blowing method for final analysis. The gas chromatograph was equipped with a DB-5MS $30\ m \times 0.25\ mm \times 0.25\ mm$ capillary column and the mass spectrometer employed a quadrupole mass filter with a 70 eV electron impact ionizer. The temperature of the programmed temperature vaporizer was held at 270 °C. The initial oven temperature was set at 40 °C for 2 min, then increased step-by-step to 150 °C (by $5\ °C\ min^{-1}$) for 5 min, 280 °C (by $10\ °C\ min^{-1}$) for 10 min, and 320 °C (by $10\ °C\ min^{-1}$) for 5 min. A pH meter (Mettler pH, S220-K) was used to measure the acidity change of DBC after the reaction. The UV−vis spectra of residual EC and extracted OC were measured using the UV−vis spectroscopy (Perkin Elmer LAMBDA 650).

Analysis and characterization of oxidizing agents and products

Thermal gravimetric analysis. The sulfur-containing species produced during diesel soot photooxidation were investigated using a combined method of thermogravimetry–mass spectrometry (TGA–MS). In brief, a Mettler-Toledo thermogravimetry system (TGA, DSC1-1600HT) was coupled with a quadrupole mass spectrometer (MS, ThermoStar- GSD/350, Pfeiffer Vacuum) by a silica capillary at a temperature of 250 °C. The MS system was equipped with an electron ionization source with the voltage at 70 eV and provided the mass spectra up to m/z 300. TGA–MS was carried out over the range 35–800 °C with a 30 K min^{-1} gradient. The whole experiment was accomplished under an inert purge gas of N_2 with a constant flow rate of 70 ml min^{-1}. In a typical desorption run, a blank test of the empty sample crucible was performed at 25 °C in an N_2 stream (the carrier gas flow rate: 50 mL min^{-1} and the shielding gas flow rate: 20 mL min^{-1}). Afterward, the sample was weighed and placed in the sample container. The pure DBC (15 mg), SO_2-aged DBC (15 mg), pure H_2SO_4 solution (60 μL), and an H_2SO_4–DBC mixture (30 μL H_2SO_4 (1.8 mol/L) and 15 mg DBC) were placed in sequence in an alumina crucible of 70 μL. The mass spectra of m/z 98, 80, 64, and 48, which correspond to the main fragment components of H_2SO_4 (H_2SO_4, SO_3, SO_2, SO, respectively), were chosen to further verify H_2SO_4 formation.

ESR measurements. An electron spin resonance spectrometer (ELEXSYS E500 ESR; Bruker) with a modulation frequency of 100 kHz and a microwave frequency of 9.5 GHz was used to capture reactive radical signals. 5-tert-butoxycarbonyl-5-methyl-1-pyrroline-N-oxide (BMPO) added to a freshly prepared 0.1 M solution in deionized water was used for capturing OH radicals in aqueous solutions. 5,5-dimethylpyrroline-N-oxide (DMPO) was used to capture superoxide ($\cdot O_2^-$). 2,2,6,6-tetramethylpiperidine-1-oxyl (TEMPO) was used to capture the photo-induced electrons in the DBC suspension. DBC suspensions loaded in a quartz capillary tube (1 mm Ø and 10 cm length) were continuously irradiated with the Xenon lamp during the monitoring of radical signals in the ESR spectrometer. The typical parameters for ESR measurement were as follows: the sweep width was 100 G, the modulation amplitude was 1.00 G, and the sweep time was 81.92 ms.

IC analysis. To quantitively the H_2SO_4 concentration under different conditions, Ion chromatography (IC, Model DIONEX ICS-2100, Thermo Scientific, Inc., USA) was employed to analyze the changes in the concentrations of water-soluble ions (such as SO_4^{2-} and NO_3^-). A certain amount of SO_4^{2-} may be contained in the primordial DBC samples due to the combustion of sulfur-containing species in fuel. Thus, DBC samples were ultrasonically extracted using ultrapure water at least 10 times to exclude interference from these preexisting SO_4^{2-} ions in the measurement of newly produced SO_4^{2-} ions during IC analysis. After the reaction finished, DBC samples (25 mg) obtained under different experimental conditions were first dispersed in 20 mL of ultrapure water and sonicated for 10 min, and subsequently filtered using a syringe filter (13 mm diameter, 0.22 μm pore-size). The filtered liquid was split in half. Half of the samples were directly analyzed by IC.

Data availability

The data that support the findings of this study are available from the corresponding author upon reasonable request. Source data are provided with this paper.

References

1. Bond, T. C. et al. A technology-based global inventory of black and organic carbon emissions from combustion. *J. Geophys. Res.-Atmos.* **109**, 2003JD003697 (2004).
2. Wang, R. et al. Black carbon emissions in China from 1949 to 2050. *Environ. Sci. Technol.* **46**, 7595–7603 (2012).
3. Kholod, N. & Evans, M. Reducing black carbon emissions from diesel vehicles in Russia: an assessment and policy recommendations. *Environ. Sci. Policy* **56**, 1–8 (2016).
4. Sahu, S. K., Beig, G. & Sharma, C. Decadal growth of black carbon emissions in India. *Geophys. Res. Lett.* **35**, 2007GL032333 (2008).
5. Jacobson, R. S., Korte, A. R., Vertes, A. & Miller, J. H. The molecular composition of soot. *Angew. Chem. Int. Ed.* **59**, 4484–4490 (2020).
6. Niessner, R. The many faces of soot: characterization of soot nanoparticles produced by engines. *Angew. Chem. Int. Ed.* **53**, 12366–12379 (2014).
7. Frank, B., Schuster, M. E., Schlogl, R. & Su, D. S. Emission of highly activated soot particulate—the other side of the coin with modern diesel engines. *Angew. Chem. Int. Ed.* **52**, 2673–2677 (2013).
8. Cao, C. et al. Urban heat islands in China enhanced by haze pollution. *Nat. Commun.* **7**, 12509 (2016).
9. Li, Z. Q. et al. Aerosol and boundary-layer interactions and impact on air quality. *Natl Sci. Rev.* **4**, 810–833 (2017).
10. Gustafsson, O. & Ramanathan, V. Convergence on climate warming by black carbon aerosols. *Proc. Natl Acad. Sci. USA* **113**, 4243–4245 (2016).
11. Khalizov, A. F., Xue, H. X., Wang, L., Zheng, J. & Zhang, R. Y. Enhanced light absorption and scattering by carbon soot aerosol internally mixed with sulfuric acid. *J. Phys. Chem. A* **113**, 1066–1074 (2009).
12. Peng, J. F. et al. Markedly enhanced absorption and direct radiative forcing of black carbon under polluted urban environments. *Proc. Natl Acad. Sci. USA* **113**, 4266–4271 (2016).
13. Ramanathan, V. & Carmichael, G. Global and regional climate changes due to black carbon. *Nat. Geosci.* **1**, 221–227 (2008).
14. Bond, T. C. et al. Bounding the role of black carbon in the climate system: a scientific assessment. *J. Geophys. Res.-Atmos.* **118**, 5380–5552 (2013).
15. Liao, H., Chang, W. Y. & Yang, Y. Climatic effects of air pollutants over China: a review. *Adv. Atmos. Sci.* **32**, 115–139 (2015).
16. George, C., Ammann, M., D'Anna, B., Donaldson, D. J. & Nizkorodov, S. A. Heterogeneous photochemistry in the atmosphere. *Chem. Rev.* **115**, 4218–4258 (2015).
17. Al-Abadleh, H. A. & Grassian, V. H. Heterogeneous reaction of NO_2 on hexane soot: a Knudsen cell and FT-IR study. *J. Phys. Chem. A* **104**, 11926–11933 (2000).
18. Han, C., Liu, Y. C. & He, H. Heterogeneous photochemical aging of soot by NO_2 under simulated sunlight. *Atmos. Environ.* **64**, 270–276 (2013).
19. Monge, M. E. et al. Light changes the atmospheric reactivity of soot. *Proc. Natl Acad. Sci. USA* **107**, 6605–6609 (2010).
20. Han, C., Liu, Y. C. & He, H. Role of organic carbon in heterogeneous reaction of NO_2 with soot. *Environ. Sci. Technol.* **47**, 3174–3181 (2013).
21. Kalberer, M., Ammann, M., Arens, F., Gaggeler, H. W. & Baltensperger, U. Heterogeneous formation of nitrous acid (HONO) on soot aerosol particles. *J. Geophys. Res.-Atmos.* **104**, 13825–13832 (1999).
22. Ammann, M. et al. Heterogeneous production of nitrous acid on soot in polluted air masses. *Nature* **395**, 157–160 (1998).
23. He, H. et al. Mineral dust and NOx promote the conversion of SO_2 to sulfate in heavy pollution days. *Sci. Rep.* **4**, 1–6 (2014).
24. Wang, G. H. et al. Persistent sulfate formation from London Fog to Chinese haze. *Proc. Natl Acad. Sci. USA* **113**, 13630–13635 (2016).
25. Wang, J. F. et al. Fast sulfate formation from oxidation of SO_2 by NO_2 and HONO observed in Beijing haze. *Nat. Commun.* **11**, 2844 (2020).
26. Liu, T. Y., Chan, A. W. H. & Abbatt, J. P. D. Multiphase oxidation of sulfur dioxide in aerosol particles: implications for sulfate formation in polluted environments. *Environ. Sci. Technol.* **55**, 4227–4242 (2021).

27. Cheng, Y. F. et al. Reactive nitrogen chemistry in aerosol water as a source of sulfate during haze events in China. *Sci. Adv.* **2**, e1601530 (2016).

28. Wang, Y. S. et al. Mechanism for the formation of the January 2013 heavy haze pollution episode over central and eastern China. *Sci. China-Earth Sci.* **57**, 14–25 (2014).

29. Zhao, Y., Liu, Y., Ma, J., Ma, Q. & He, H. Heterogeneous reaction of SO_2 with soot: the roles of relative humidity and surface composition of soot in surface sulfate formation. *Atmos. Environ.* **152**, 465–476 (2017).

30. He, G. Z., Ma, J. Z. & He, H. Role of carbonaceous aerosols in catalyzing sulfate formation. *ACS Catal.* **8**, 3825–3832 (2018).

31. He, G. & He, H. Water promotes the oxidation of SO_2 by O_2 over carbonaceous aerosols. *Environ. Sci. Technol.* **54**, 7070–7077 (2020).

32. Zhang, F. et al. An unexpected catalyst dominates formation and radiative forcing of regional haze. *Proc. Natl Acad. Sci. USA* **117**, 3960–3966 (2020).

33. Yao, L. et al. Unprecedented ambient sulfur trioxide (SO_3) detection: possible formation mechanism and atmospheric implications. *Environ. Sci. Technol.* **7**, 809–818 (2020).

34. Li, M. et al. Role of elemental carbon in the photochemical aging of soot. *Proc. Natl Acad. Sci. USA* **115**, 7717–7722 (2018).

35. Zhu, J. L., Shang, J., Chen, Y. Y., Kuang, Y. & Zhu, T. Reactive oxygen species-related inside-to-outside oxidation of soot particles triggered by visible-light irradiation: physicochemical property changes and oxidative potential enhancement. *Environ. Sci. Technol.* **54**, 8558–8567 (2020).

36. Han, C., Liu, Y. C., Ma, J. Z. & He, H. Key role of organic carbon in the sunlight-enhanced atmospheric aging of soot by O_2. *Proc. Natl Acad. Sci. USA* **109**, 21250–21255 (2012).

37. Zhu, J. L., Shang, J. & Zhu, T. A new understanding of the microstructure of soot particles: The reduced graphene oxide-like skeleton and its visible-light driven formation of reactive oxygen species. *Environ. Pollut.* **270**, 116079 (2021).

38. Zhang, G. H. et al. Black carbon involved photochemistry enhances the formation of sulfate in the ambient atmosphere: evidence from in situ individual particle investigation. *J. Geophys. Res.-Atmos.* **126**, e2021JD035226 (2021).

39. Zhang, D. & Zhang, R. Y. Laboratory investigation of heterogeneous interaction of sulfuric acid with soot. *Environ. Sci. Technol.* **39**, 5722–5728 (2005).

40. Drewnick, F., Diesch, J. M., Faber, P. & Borrmann, S. Aerosol mass spectrometry: particle-vaporizer interactions and their consequences for the measurements. *Atmos. Meas. Tech.* **8**, 3811–3830 (2015).

41. Jimenez, J. L. et al. Ambient aerosol sampling using the aerodyne aerosol mass spectrometer. *J. Geophys. Res.-Atmos.* **108**, 8245 (2003).

42. Smith, O. I. & Stevenson, J. S. Determination of cross-sections for formation of parent and fragment ions by electron-impact from SO_2 and SO_3. *J. Chem. Phys.* **74**, 6777–6783 (1981).

43. Li, C., Chen, X., Shen, L. M. & Bao, N. Z. Revisiting the oxidation of graphite: reaction mechanism, chemical stability, and structure self-regulation. *Acs. Omega* **5**, 3397–3404 (2020).

44. Dimiev, A. M., Bachilo, S. M., Saito, R. & Tour, J. M. Reversible formation of ammonium persulfate/sulfuric acid graphite intercalation compounds and their peculiar Raman spectra. *ACS Nano* **6**, 7842–7849 (2012).

45. He, G. et al. Generation and release of oh radicals from the reaction of H_2O with O_2 over soot. *Angew. Chem. Int. Ed.* **134**, e202201638 (2022).

46. Xu, M. J. et al. Unveiling the role of defects on oxygen activation and photodegradation of organic pollutants. *Environ. Sci. Technol.* **52**, 13879–13886 (2018).

47. Zhao, H. X. et al. Photoinduced formation of reactive oxygen species and electrons from metal oxide-silica nanocomposite: an EPR spin-trapping study. *Appl. Surf. Sci.* **416**, 281–287 (2017).

48. Zhao, Y. C., Liu, Y., Zhang, X. B. & Liao, W. C. Environmental transformation of graphene oxide in the aquatic environment. *Chemosphere* **262**, 127885 (2021).

49. Hou, W. C. et al. Photochemical transformation of graphene oxide in sunlight. *Environ. Sci. Technol.* **49**, 3435–3443 (2015).

50. Yuan, Y. C. et al. Quantum dot photocatalysts for organic transformations. *J. Phys. Chem. Lett.* **12**, 7180–7193 (2021).

51. Kampouri, S. & Stylianou, K. C. Dual-functional photocatalysis for simultaneous hydrogen production and oxidation of organic substances. *ACS Catal.* **9**, 4247–4270 (2019).

52. Liu, W. et al. Visible-light-driven photocatalytic degradation of diclofenac by carbon quantum dots modified porous g-C3N4: mechanisms, degradation pathway and DFT calculation. *Water Res.* **150**, 431–441 (2019).

53. Song, H. et al. Selective photo-oxidation of methane to methanol with oxygen over dual-cocatalyst-modified titanium dioxide. *ACS Catal.* **10**, 14318–14326 (2020).

54. Su, C. L. et al. Probing the catalytic activity of porous graphene oxide and the origin of this behaviour. *Nat. Commun.* **3**, 1298 (2012).

55. Tsona, N. T. & Du, L. A potential source of atmospheric sulfate from O_2-induced SO_2 oxidation by ozone. *Atmos. Chem. Phys.* **19**, 649–661 (2019).

56. Tsona, N. T., Li, J. & Du, L. From O_2-initiated SO_2 oxidation to sulfate formation in the gas phase. *J. Phys. Chem. A* **122**, 5781–5788 (2018).

57. Radi, R. Oxygen radicals, nitric oxide, and peroxynitrite: redox pathways in molecular medicine. *Proc. Natl Acad. Sci. USA* **115**, 5839–5848 (2018).

58. Wang, Y. B., Zhao, X., Cao, D., Wang, Y. & Zhu, Y. F. Peroxymonosulfate enhanced visible light photocatalytic degradation bisphenol A by single-atom dispersed Ag mesoporous g-C3N4 hybrid. *Appl. Catal. B-Environ.* **211**, 79–88 (2017).

59. Gao, H. Y. et al. First direct and unequivocal electron spin resonance spin-trapping evidence for pH-dependent production of hydroxyl radicals from sulfate radicals. *Environ. Sci. Technol.* **54**, 14046–14056 (2020).

60. Liu, X. J. et al. $Cu_2In_2ZnS_5/Gd_2O_2S$: Tb for full solar spectrum photoreduction of Cr (VI) and CO_2 from UV/vis to near-infrared light. *Appl. Catal. B-Environ.* **249**, 82–90 (2019).

61. Yao, L. et al. Atmospheric new particle formation from sulfuric acid and amines in a Chinese megacity. *Science* **361**, 278–281 (2018).

62. Kulmala, M. et al. Is reducing new particle formation a plausible solution to mitigate particulate air pollution in Beijing and other Chinese megacities? *Faraday Discuss.* **226**, 334–347 (2021).

63. Cappa, C. D. et al. Radiative absorption enhancements due to the mixing state of atmospheric black carbon. *Science* **337**, 1078–1081 (2012).

64. Jacobson, M. Z. Strong radiative heating due to the mixing state of black carbon in atmospheric aerosols. *Nature* **409**, 695–697 (2001).

65. Gustafsson, O. et al. Brown clouds over South Asia: biomass or fossil fuel combustion? *Science* **323**, 495–498 (2009).

66. Zhang, R. Y. et al. Variability in morphology, hygroscopicity, and optical properties of soot aerosols during atmospheric processing. *Proc. Natl Acad. Sci. USA* **105**, 10291–10296 (2008).

67. Liu, D. T. et al. Black-carbon absorption enhancement in the atmosphere determined by particle mixing state. *Nat. Geosci.* **10**, 184–U132 (2017).

68. Ma, Q., Wang, L., Chu, B., Ma, J. & He, H. Contrary role of H_2O and O_2 in the kinetics of heterogeneous photochemical reactions of SO_2 on TiO_2. *J. Phys. Chem. A* **123**, 1311–1318 (2019).

69. Yang, W. W. et al. The effect of water on the heterogeneous reactions of SO_2 and NH_3 on the surfaces of alpha-Fe_2O_3 and gamma-Al_2O_3. *Environ. Sci.-Nano* **6**, 2749–2758 (2019).

Author contributions

H.H. designed and supervised the research. P.Z. designed and performed the experiments. Q.M. gave guidance for the experimental research. T.C., Q.M., B.C., Y.W., Y.M, and Y.Y. provided suggestions for the manuscript. P.Z. and H.H. wrote the manuscript. All authors discussed the results and commented on the manuscript.

Competing interests

The authors declare no competing interests.

Additional information

Supplementary information The online version contains supplementary material available at
https://doi.org/10.1038/s41467-022-33120-3.

Correspondence and requests for materials should be addressed to Qingxin Ma or Hong He.

Peer review information *Nature Communications* thanks Markku Kulmala and the other, anonymous, reviewers for their contribution to the peer review of this work. Peer reviewer reports are available.

Reprints and permission information is available at
http://www.nature.com/reprints

Publisher's note Springer Nature remains neutral with regard to jurisdictional claims in published maps and institutional affiliations.